Ranscriptome Analysis Reveals the Molecular Mechanism of Yiqi Rougan Decoction in Reducing CCl4-induced Liver Fibrosis in Rats

Yu Xiong
Chongqing Medical University
Jinyuan Hu
Chongqing Medical University
Chen Xuan
Chongqing Medical University
Jiayu Tian
Chongqing Medical University
Kaiyue Tan
Chongqing Medical University
Zhiwei Chen
Chongqing Medical University
Yan Luo
Chongqing Medical University
Xuqin Du
Chongqing Medical University
Junxiong Cheng
Chongqing Medical University
Lanyue Zhang
Chongqing Medical University
Wenfu Cao (caowenfu9316@163.com)
Chongqing Medical University

Research Article

Keywords: Yiqi Rougan decoction, liver fibrosis, RNA sequencing, endoplasmic reticulum stress, apoptosis, autophagy

Posted Date: October 8th, 2021

DOI: https://doi.org/10.21203/rs.3.rs-919251/v1

Abstract

Background

Liver fibrosis develops from various chronic liver diseases, and there is currently a lack of specific treatment strategies. Yiqi Rougan decoction (YQRG) is a traditional Chinese medicine that has shown durative effects in the treatment of liver fibrosis; however, the mechanism associated with YQRG-related improvements in liver fibrosis remains to be experimentally determined. This study evaluated the therapeutic effect of YQRG on carbon tetrachloride (CCl_4)-induced liver fibrosis in rats and its molecular mechanism.

Methods

We used low-, medium-, and high-dose YQRG to treat CCl_4-induced liver fibrosis in rats, followed by assessment of liver injury and fibrosis according to liver appearance, body weight, liver mass index, histopathologic examination, and serum testing. Additionally, we performed transcriptome analysis using RNA-sequencing (RNA-seq) technology, including cluster, Gene Ontology (GO), and pathway analyses, to identify differentially expressed genes (DEGs), and protein and gene expression were detected by immunofluorescence (IFC), western blot, and real-time quantitative PCR.

Results

The results showed that YQRG effectively alleviated CCl_4-induced liver injury and fibrosis in rats, including observations of improved liver function, decreased activity of hepatic stellate cells (HSCs), and decreased extracellular matrix (ECM) deposition. Moreover, we identified downregulated and upregulated DEGs in the model group relative to the control and YQRG-treated groups, with GO analysis revealing their enrichment in biological processes, such as endoplasmic reticulum stress (ERS), apoptosis, and autophagy. Furthermore, pathway analysis showed that YQRG treatment downregulated the mitogen-activated protein kinase (MAPK) and phosphoinositide 3-kinase/Akt (PI3K/AKT) signalling pathways and upregulated other signalling pathways, including those related to peroxisome proliferator-activated receptors(PPAR) and AMP-activated protein kinase(AMPK), with these finding subsequently verified experimentally.

Conclusion

These findings showed that YQRG improved CCl_4-induced liver fibrosis through multiple mechanisms and pathways, offering critical insight into the YQRG-related therapeutic mechanism and promoting further research into its potential application.

Background

Hepatic fibrosis is an abnormal wound-healing process in which hepatic parenchymal cells (HPCs) transform into fibrous tissue of ECM [1-3], which is detrimental to human health. Liver fibrosis can subsequently evolve into liver cirrhosis and hepatocellular carcinoma, which account for 3.5% of global annual mortality [4]. It is difficult to accurately calculate the prevalence of liver fibrosis [5,6] and generally believed that the condition is reversible. Therefore, actively reversing liver fibrosis is particularly important to the prevention and treatment of chronic liver disease. Notably, there is no specific anti-fibrosis therapy [7], making research supporting the active development of safe and effective anti-fibrosis drugs a significant undertaking to reveal their molecular mechanism.

Activation of resting HSCs represents the critical mechanism associated with liver fibrosis formation [8-10]. Additionally, ERS describes the response to continuous aggregation of unfolded or misfolded proteins in the ER, which alters ER homeostasis [11], induces HPCs apoptosis and reportedly promotes the formation of liver fibrosis [12,13]. Moreover, apoptosis of HPCs, which can promote the transformation of HSCs from a static to an activated state, supports fibrotic initiation [14,15]. Previous studies report that increased autophagy and levels of unfolded proteins can occur after the loss of cellular homeostasis, with these processes also implicated in the occurrence of fibrosis [16]. Furthermore, recent studies show that continuous ERS can activate autophagy, which subsequently promotes the activation of resting HSCs and induces liver fibrosis [17,18].

Current treatment modalities for liver fibrosis mainly focus on eliminating the risk factors that are known to progressively decline into end-stage liver fibrosis, and treatment of end-stage liver fibrosis mainly involves liver transplantation, which carries the risk of trauma and rejection. Recently, the use of mesenchymal stem cell therapy for hepatic fibrosis has emerged, although there exists a risk of carcinogenesis. Therefore, it is particularly important to identify safe and effective anti-fibrosis therapies.

Traditional Chinese medicine has unique advantages in the treatment of chronic liver disease, especially in reducing hepatocyte damage, inhibiting inflammation, and promoting anti-fibrosis effects [20]. Yiqi Rougan (YQRG) decoction is a traditional Chinese medicine. Due to the complexity of traditional Chinese medicine prescriptions, the mechanism of action of YQRG in treating liver fibrosis remains misunderstood, including associated changes in gene expression. Transcriptome analysis using RNA-seq technology can potentially elucidate the molecular mechanism of disease occurrence [21]. In the present study, we analysed the main components of YQRG by ultra-high performance liquid chromatography with quadrupole time-of-flight mass spectrometry (UHPLC-QTOF-MS), evaluated its effects on liver function and fibrosis in a rat model of CCl_4-induced liver fibrosis, and identified DEGs in rat liver following YQRG treatment.

Methods

Drugs and materials

YQRG was purchased from the Department of Traditional Chinese Medicine at the First Affiliated Hospital of Chongqing Medical University (Chongqing, China). CCl_4 (batch no. c805329) and olive oil (batch no. o815210) were purchased from Shanghai McLean Biochemical Technology Co., Ltd. (Shanghai, China). Kits for assessing alanine aminotransferase (ALT; batch no. s03030) and aspartate aminotransferase (AST; batch no. s03040) kit were purchased from Shenzhen Redu Life Technology Co., Ltd. (Shenzhen, China), a kit for assessing hydroxyproline (HYP; batch no. a030-3-1) kit was purchased from Nanjing Jiancheng Bioengineering Institute (Nanjing, China), and colchicine (batch no. h20113208) was purchased from Guangdong Bidi Pharmaceutical Co., Ltd. (Guangdong, China). Enzyme-linked immunosorbent assay (ELISA) kits for hyaluronic acid (HA batch no. qz-25723), laminin (LN; batch no. qz-25677), type IV collagen (IV-C; batch no. qz-25741), type III procollagen (PC-III; batch no. qz-20116), rat caspase 12 (CASP12; batch no. qz-20065), C/EBP homologous protein (CHOP; batch no. qz-25805), activated transcription factor 6 (ATF6; batch no. qz-25812), inositolase 1 (IRE1; batch no. qz-25833), phosphorylated (p)-extracellular signal-regulated kinase (PERK;batch no. qz-25829), immunoglobulin-binding protein (BiP; batch no. qz-25818) were obtained from Quanzhou Jiubang Biological Technology Co., Ltd. (Quanzhou, China). Trizol (batch no. 108-95-2), the Primescript RT kit and gDNA eraser (batch no. rr047a) were obtained from Takara Bio (Shiga, Japan). Primers for quantitative (q)PCR were provided by Qingke Biotechnology (Beijing, China). Antibodies against α-smooth muscle actin (α-SMA; 19245), p38 (8690), p-p38 (4511), AMPK(2532), p-AMPK (2535), and β-actin (4970) were obtained from Cell Signaling Technology (Danvers, MA, USA). Antibodies against light-chain (LC)3-I/II (ab128025) and LC3-II (ab192890) were obtained from Abcam (Cambridge, UK). Terminal deoxynucleotidyl transferase dUTP nick end labelling (TUNEL) staining kits (batch no. g1501) were purchased from Wuhan Seville Biotechnology Co., Ltd. (Wuhan, China). Acetonitrile, methanol, and formic acid (LC-MS grade) were obtained from CNW Technology (Dusseldorf, Germany).

YQRG preparation

YQRG contains eight herbs: *Astragalus mongholicus Bunge, Atractylodes Macrocephala Koidz, Salvia miltiorrhizae Bunge, Curcuma longa L, Paeonia lactiflora Pall, Cyperus rotundus L, Sargassum fusiforme Setch and Trichosanthes Kirilowii Maxim*. The herbal information and composition ratio are shown in Table 1. According to the surface area conversion ratio between rats and humans (6.3), we calculated the low-, medium-, and high-dose YQRG concentrations for use in rats at 4.95 g/kg, 9.9 g/kg, and 19.8 g/kg, respectively. According to this dosage, the Chinese herbs described were submerged in distilled water for 30 min, decocted three times, filtered, and concentrated three times to create YQRG Decoction at low, medium, and high dosages [22]. The composition of YQRG was determined by UHPLC-QTOF-MS for quality control.

UHPLC-QTOF-MS analysis

A methanol:water extract (4:1, v/v) was added to the YQRG Decoction (150 μL) and vortexed for 30 s, followed by sonication for 1 h in an ice water bath before incubation at −40°C for 1 h and centrifugation at 12,000 rpm at 4° for 15 min. The supernatant was then passed through a 0.22-μm filter membrane for

UHPLC tandem MS (MS/MS) analysis (Infinity 1290; Agilent Technology, Santa Clara, CA, USA). Mobile phases A and B comprised water with 0.1% formic acid and acetonitrile with 0.1% formic acid, respectively, and were passed at a flow rate of 400 μL/min. The sample (5 μL) was injected onto the Waters C18 column (1.7 × 2.1 μm × 100 mm; Waters Corp., Milford, MA, USA), followed by gradient elution: 0–3.5 min (5–15% B), 3.5–6 min (15–30% B), 6–12 min(30–70% B), 12–18 min (70–100% B), and 18–25 min (100% B).. High resolution MS/MS was performed using a Q precision mass spectrometer (Thermo Fisher Scientific, Waltham, MA, USA), with the data analysed using Xcalibur software (Thermo Fisher Scientific).

Animal experiments

Male Sprague–Dawley rats (n = 56; 180–220 g) were purchased from the Experimental Animal Center of Chongqing Medical University. Animal experiments were conducted in a specific pathogen-free animal laboratory (syxk 2018-0003) at the Experimental Animal Center according to the Guidelines for the Care and Use of Experimental Animals from the National Institutes of Health (Bethesda, MD, USA). The experiments were approved by the Ethics Committee of Chongqing Medical University. After 1 week of adaptive feeding, rats were randomly divided into two groups: the control (n = 8) and the CCl_4-treatment group (n = 48). Rats in the CCl_4-treatment group received intraperitoneal (i.p.) injection of 50% CCl_4–olive oil solution (1 mL/kg) twice weekly for 9 weeks. At the end of the 4^{th} week, rats in CCl_4-treatment group were randomly divided into four groups: low, medium, and high-dose treatment groups (n = 12) received YQRG at 4.95 g/kg/day, 9.9 g/kg/day, and 19.8 g/kg/day, respectively; and the model group (n = 12) received saline for 5 weeks. At the end of the 9^{th} week, rats were anaesthetized by i.p. injection of 2% pentobarbital sodium and asphyxiated with high-concentration CO_2. Blood was collected from the abdominal aorta, and the liver was removed immediately and the weight recorded. Liver tissue was quickly cut into pieces for subsequent liver haematoxylin and eosin (H&E) and Masson staining, immunohistochemistry (IHC), immunofluorescence staining, and transmission electron microscopy (TEM) analysis. The remaining tissues and serum were stored at -80°C until further use.

liver index, Serum biochemical and liver HYP analyses

During the animal experiments, all rats were weighed and recorded every 2 weeks. Following liver removal and weighing, the liver index was calculated according to the body weight and liver weight to evaluate liver injury, as follows: Liver index = (liver weight / body weight) × 100. According to their respective manufacturer instructions, Serum ALT, AST levels and liver HYP content were measured with kits, Configure the working reagent, load the sample, set the parameters in an automatic biochemical analyzer (Shenzhen Redu Life Technology Co., Ltd.) and put it on the computer for detection.

Histologic analysis

Liver tissue was fixed with 4% paraformaldehyde for 24 h, dehydrated, embedded in paraffin, and sliced (4 μm), followed by staining with H&E and Masson Staining. For H&E staining, the slices were dewaxed

first, soaked with hematoxylin dye solution for 10 min, then washed with distilled water. After differentiation, the slices were rinsed again, and then rinsed with blue-returning solution. Soak the slices in ethanol (85% and 95%) for 5 min, and infect the slices in eosin dye for 10 min. After dehydration for 5 min (ethanol and xylene). In addition, for Masson staining, the dewaxed slices were placed in Masson A for 15 h and then rinsed. The Masson mixture (Masson B:Masson C=1:1) was soaked for 1 min and washed. The mixture was differentiated with 1% hydrochloric acid alcohol for 1min and washed. The tissue turned red after Masson D treatment for 6 min. The slices were rinsed, differentiated, dehydrated and sealed with 1% glacial acetic acid. In the end,Tissue sections were then observed and images obtained using an optical microscope (BX53; Olympus, Tokyo, Japan).

IHC analysis

Paraffin sections were dewaxed, and citric acid antigen repair buffer was soaked to repair the antigen. The antigen was incubated with 3% hydrogen peroxide solution for 25 min, washed with phosphate-buffered saline (PBS), and sealed with 3% bovine serum albumin (BSA) at room temperature for 30 min. The antibody was incubated with anti-α-SMA and HRP-conjugated secondary antibodies, followed by DAB staining, rinsed, sectioned with differentiation solution, dehydrated with ethanol and xylene, and sealed with neutral rubber. followed by washing, observation, and imaging using a microscope (BX53; Olympus).

Assessment of ultrastructural morphology

Liver tissue was cut into 1 mm^3 immediately upon collection of the liver (within 1 min - 2 min), fixed in 2.5% glutaraldehyde, and washed with 1 M PBS, 1% osmic acid was added to the sections for a 2 h incubation, washed, dehydrated, penetrated, dehydrated with ethanol and acetone, and then embedded with 812 embedding agent. The embedding plate was polymerized for 48 h, and the resin block was placed in the ultra-thin slicer (60 nm – 80 nm). Stained, washed and dried with 2% uranium acetate saturated alcohol and 2.6% lead citrate solution. followed by observation of the ultrastructure of the liver and collection of images via TEM (JEM-1400plus; JEOL, Tokyo, Japan).

RNA-seq analysis

RNA-seq was performed and sequencing libraries were constructed using the Novaseq 6000 platform and the TruseqTM RNA sample prep kit (Illumina, San Diego, CA, USA). Total RNA was extracted with Trizol reagent, and mRNA was separated using oligo(DT) magnetic beads and randomly broken into small fragments. Six-base random primers were used to reverse transcribe cDNA, followed by end repair and sequencing. Changes in gene expression in liver tissue following YQRG treatment were assessed according to the identification of DEGs (fold changes >2 or <−2; false discovery rate < 0.05). DEGs were clustered and analysed using the GO database and Kyoto Encyclopedia of Genes and Genomes (KEGG; http://www.genome.jp/kegg/) pathway analysis.

Network construction and analysis

The STRING database (https://string-db.org/) is a database commonly used to predict protein-protein interaction (PPI), The main DEG was entered into the string database, the interaction score was set to ≥ 0.9 and the species was selected as "Homo sapiens" to create PPI network. Then, the results were saved and exported in TSV format. Cytoscape (v.3.6.0; https://cytoscape.org/) was used to visualize the PPI networks. The TSV format file is imported into Cytoscape for PPI visualization.

Double immunofluorescence staining

Double immunofluorescence staining was performed to detect colocalization of TUNEL staining and a-SMA. Additionally, LC3-II and a-SMA were also examined. For the former staining, The slices were dewaxed into xylene, ethanol, and distilled water, respectively, and then circled into protease K working solution and incubated at 37℃ for 22 min. PBS was washed and 0.1% Triton was added for 20 min at room temperature. Then, the buffer was incubated at room temperature for 10 min. TUNEL kit reaction solution (TDT enzyme :dUTP: Buffer =1:5:50) was added into the ring and incubated for 2 h at 37℃, and sealed with 3% BSA for 30min. Sections were incubated with rabbit anti-α-SMA at 4℃ overnight, and then FITC-conjugated goat anti-rabbit IgG (Wuhan Service Biotechnology Ltd.) was used for 50 min at ambient temperature, dark. followed by nucleus staining with 4',6-diamino-2-phenylindole (DAPI; Wuhan Service Biotechnology Ltd.) for 10 min. Additionally, For the latter staining, sections were dewaxed, immersed in EDTA antigen repair buffer, circled, and sealed with 3% hydrogen peroxide and 3% BSA, respectively. Rabbit anti-LC3-II was added and incubated overnight, followed by FITC-Conjugated goat Anti-Rabbit IgG, then cy3-TSA was added for 10 min, washed, and antigen repair was performed again. In incubated with the primary antibodies (anti-α-SMA), followed by FITC-conjugated goat anti-Rabbit IgG, DAPI staining was used. Sections were then observed and images were obtained by fluorescence microscopy (eclipse CI; Nikon, Tokyo, Japan).

ELISA

ELISA was performed according to the manufacturer instructions for the ELISA kit. Levels of HA, LN, PC-III, IV-C, CASP12, CHOP, ATF6, IRE1, PERK and BiP in liver tissue were quantified. PBS was added to liver tissue for homogenization, followed by centrifugation at 4°C for 20 min. This process was repeated three times, and the supernatant was then used for ELISA detection. Add the sample and standard, wash the plate, add the antibody to be tested for incubation, wash the plate again, incubate with enzyme solution, wash the plate, develop the colour of TMB substrate, add 50 uL and 450um reading of termination solution, and finally calculate its concentration.

Real-time qPCR

We then detected mRNA levels of *Acta2* (encoding α-SMA) , *Hspa5* (encoding BiP), *Eif2ak3* (encoding PERK), *Atf6*, *Ern1* (encoding IRE1), *Chop*, *Casp12*, *B-cell lymphoma-2* (*Bcl-2*), *Lc3b*, *unc-51-like autophagy-activating kinase 1* (*Ulk1*), *tissue inhibitor of metalloproteinase 1* (*Timp1*), *metalloproteinase 9* (*Mmp9*), *P38*, and *Ampk*. Weigh 100 mg liver tissue, add 2 mL trail homogenate, centrifuge at 12000 rpm for 10 min, collect 700 uL supernatant, add 140 uL chloroform (supernatant: chloroform= 1:0.2), mix

well, centrifuge, take 300 uL supernatant, add 300 uL isopropanol, shake for 1 min, remove the liquid, add 75% ethanol, wash and separate the heart, dry after absorbing the ethanol, add dH_2O, measure and adjust the sample concentration, cDNA was synthesized by reverse transcription with PrimeScript RT reagent Kit with gDNA Eraser (Takara Bio). PCR amplification was then performed under the following cycling conditions: 95°C pre-denaturation for 10 min, 95°C dena-turation for 15 s, 60°C annealing for 1 min, with a total of 40 cycles (CFX96, Bio-Rad). *β-Actin* was used as a control for normalization of gene expression, and fold changes were calculated using the $2^{-\Delta\Delta CT}$ method. The primer sequences are shown in Table 2.

Western blot

Proteins were extracted from liver tissue with Radioimmunoprecipitation buffer containing a protease inhibitor and phosphatase inhibitor. Proteins were separated by electrophoresis, followed by transfer to polyvinylidene fluoride membranes. Membranes were washed five times with Tris-buffered saline containing Tween-20 (TBST) and incubated overnight at 4°C with respective primary antibodies [α-SMA (1:1000), LC3-I/II (1:1000), p38 (1:1000), p-p38 (1:1000), AMPK (1:1000), p-AMPK (1:1000)and β-actin (1:1000)]. The membrane was then washed five times with TBST and incubated with HRP-conjugated secondary antibody(Boster Bio) for 1 h. Bands were visualized by enhanced chemiluminescence and images obtained using a chemiluminescence imaging system (Odyssey FC; Licor Biosciences, Lincoln, NE, USA). ImageJ software (National Institutes of Health, Bethesda, MD, USA) was used for data analysis.

Statistical analysis

Data represent the mean ± standard deviation. Statistical analysis was performed using SPSS 25.0 software (IBM, United States) .(v.8.0.2; GraphPad Software, San Diego, CA, USA). One-way analysis of variance and Nonparametric test were used to compare differences between groups. $p < 0.05$ was considered significant. Image production was completed by GraphPad Prism 8.0.2 Software(San Diego, CA, United States).

Results

Component analysis of YQRG

We analysed the main compounds of YQRG by UHPLC-MS/MS. Positive (Fig. 1a) and negative (Fig. 1b) ion chromatograms represented the YQRG compounds, revealing 10 main compounds (*L-Phenylalanine, Paeoniflorin, Bisdemethoxycurcumin, Curcumin, Cryptotanshinone, citric acid, Gallic acid, Protocatechualdehyde, Rosmarinic acid, Salvianolic acid A*) (Fig. 1c).

YQRG improves liver injury *in vivo*

To evaluate the effect of YQRG on liver fibrosis, we established a rat model of liver fibrosis according to the reported protocol [23]. During animal experiments, compared with the model group, the weight of rats receiving low, medium and high concentrations of YQRG (YQRG-L, YQRG-M, and YQRG-H) increased

significantly (Fig. 2a). The liver weight ratio (LW: BW) used to evaluate liver injury showed that the LW: bw ratio decreased significantly in the YQRG treatment group (Fig. 2b). Next, we measured the levels of serum ALT and AST in rats to evaluate liver function. The results showed that the levels of ALT and AST in the model group increased significantly. Surprisingly, after YQRG treatment, the levels of ALT and AST decreased and were consistent with the normal levels (Fig. 2c and d). Then, we evaluated the morphological changes of cells in liver tissue from different angles by renal appearance, H&E staining and TEM. In rats receiving CCl_4, the appearance of the liver was enlarged, abnormal, severe swelling and degeneration, and inflammatory cell infiltration. In contrast, YQRG -H well improved this pathological change (Fig. 2e). Transmission electron microscopy analysis showed that the hepatocyte structure was damaged after CCl_4-induced, including mitochondrial swelling, endoplasmic reticulum damage and bile duct dilatation. The tissue image of the YQRG H group showed an improvement in pathological damage (Fig. 2e). These results suggest that YQRG can effectively resist CCl_4-induced liver injury in rats induced by carbon tetrachloride.

YQRG resists CCl_4-induced liver fibrosis *in vivo*

Next, We then performed multiple methods to evaluate the effect of YQRG against liver fibrosis. Masson staining showed that collagen fibres (blue) accumulated after CCl_4-induced, resulting in more fibre spacing, while collagen fibres and fibre spacing decreased in the YQRG-H group (Fig. 3a). Due to HSCs activation promotion α-SMA expression, we evaluated liver injury and after treatment Changes in α-SMA levels. IHC results showed that the YQRG-H group reduced the positive expression of the model group (Fig. 3a). In addition, the fibrosis markers in the model group showed that the levels of HA, LN, PC-III and IV-C were significantly higher than those in the YQRG-H group (Fig. 3b). In addition, as the main component of collagen, the level of HYP in the model group increased but decreased after treatment with YQRG-H (Fig. 3c). As shown in Fig. 3d-f shows that the results of α-SMA expression support the immunohistochemical results in Western blot and qPCR. In addition, hepatic fibrosis is accompanied by an imbalance in ECM synthesis and degradation. ECM is regulated by TIMPs (promote ECM synthesis) and MMPs (promote ECM degradation) [24]. We analyzed the mRNA expression of *TIMP1* and *MMP9* in the liver by qPCR. The results showed that compared with the model group, the level of *MMP9* in the YQRF-H group increased significantly and the expression of *TIMP1* decreased (Fig. 3g and h). These data show that YQRG-H processing reduces the accumulation of ECM. In conclusion, these results suggest that YQRG-H treatment reduces CCl_4 induced liver fibrosis in rats.

Gene expression analysis by RNA-seqp

To gain insight into the molecular mechanism associated with YQRG-mediated improvements in liver fibrosis *in vivo*, we performed RNA-seq analysis of samples from control, model, and YQRG-H-treated rats. We identified 2689 upregulated and 2545 downregulated DEGs in the control versus model group, whereas the model versus YQRG-H group revealed 2543 upregulated and 2476 downregulated DEGs (Fig. 4a). The model group both upregulated the genes of the normal control group and YQRG-H group, and both downregulated the genes of the normal control group and YQRG-H group, which are the DEGs of

YQRG in the treatment of CCl_4 induced liver fibrosis, that is, 2141 YQRG upregulated DEGs and 2038 YQRG downregulated DEGs (Fig. 4b). Interestingly, these DEGs showed significant intergroup differences (Fig. 4c).

GO/KEGG enrichment analyses and construction of PPI network

GO enrichment analysis of the upregulated DEGs identified roles in biological processes (regulation of L-kynurenine metabolism and fatty acid oxidation, tryptophan metabolism, and branched-chain amino acid metabolism) (Fig. 5a). Downregulated DEGs were mainly involved in biological processes involving positive regulation of epithelial-to-mesenchymal transition, response to topological error protein, response to unfolded protein, regulation of ERS, autophagy, regulation of the apoptotic signalling pathway (Fig. 5b). KEGG pathway enrichment analysis showed that upregulated DEGs were associated with the peroxisome, complement, and coagulation cascade; cytochrome P450 metabolism of exogenous substances, and peroxisome proliferator-activated receptor signalling (Fig. 5c), whereas downregulated DEGs were associated with protein processing, MAPK signalling, PI3K/Akt signalling, tumour necrosis factor signalling in the ER (Fig. 5d). Notably, GO analysis identified biological processes related to YQRG treatment of liver fibrosis involved with ERS, apoptosis, and autophagy (Fig. 5e). The identified signal pathways and related genes of the first 15 closely related to liver fibrosis were plotted (Fig. 4f). The PPI network and visualization were constructed involving DEGs of ERS, apoptosis, and autophagy (Fig. 5g and h). Furthermore, the construction of a PPI network identified 33 target DEGs in Table 3.

YQRG treatment alleviates ERS *in vivo*

The inhibition of ERS is related to the improvement of liver fibrosisN [25]. As shown in Fig. 6a, we can see the formation mechanism of ERS. Transcriptome analysis of go and KEGG showed that they were enriched in endoplasmic reticulum stress-related genes and pathways. BiP, PERK, ATF6, IRE1 and CHOP are considered to be important markers of ERS[25]. To evaluate the effect of YQRG treatment on ERS, we detected changes in the expression of ERS-related markers BiP, ATF6, PERK, IRE1, and CHOP by ELISA and qPCR. Consistent with the RNA-seq results, BiP, PERK, ATF6, IRE1, and CHOP protein and mRNA levels in the model group were significantly higher than those in the control group, indicating that CCl_4 administration induced ERS. However, YQRG-H treatment reversed these changes, resulting in levels similar to those in controls (Fig. 6b–k), and leading to reductions in ERS. These findings suggested that YQRG-H treatment effectively alleviated ERS.

YQRG treatment regulates cell apoptosis

Cells apoptosis promote the occurrence of liver fibrosis, and this process is very complex (Fig. 7a.) We performed TUNEL and α-SMA (a marker for the activation of HSCs [26]) double immunofluorescence staining in liver tissues to evaluate the effect of YQRG treatment on cell apoptosis. The results showed an increased number of apoptotic cells in the model group relative to the control group along with a significant increase in the expression of α-SMA. however, YQRG-H treatment significantly reduced the number of apoptotic cells and a-SMA expression levers in the model group (Fig. 7b). Next, the expression

of apoptosis-related proteins in liver tissue was detected by ELISA and qPCR. CASP12 and BCL-2 are apoptosis-related markers and play an important role in apoptosis [27]. According to ELISA and qPCR analysis, the expression of CASP12 in CCl_4 induced group increased significantly. In contrast, the YQRG-H treatment decreased the expression level of CASP12 (Fig. 7c-d). Similarly, compared with the model group, the expression of BCL-2 in the YQRG-H group increased (Fig. 7e). These results suggest that YQRG-H treatment inhibits apoptosis.

YQRG treatment regulates autophagy *in vivo*

Autophagy is a metabolic process that is closely related to liver fibrosis (Fig. 8a). To determine whether YQRG-H treatment affects autophagy, we evaluated autophagic flux by double immunofluorescence staining, western blot, and qPCR. LC3-II is a marker for autophagy [28], double immunofluorescence staining of LC3-II and α-SMA revealed that YQRG-H treatment reduced the fluorescence signals of LC3-II and α-SMA in the model group (Fig. 8b). this result suggested autophagy activation was closely related to HSCs activation in the model group. Additionally, western blot and qPCR analyses confirmed the increased expression of LC3-II protein and mRNA in the model group, whereas these levels were decreased following YQRG-H treatment (Fig. 8c-e). ULK1 is also an important indicator regulating autophagy [29], qPCR analysis of *Ulk1* in the model group was significantly lower than that in the control group and YQRG-H groups (Fig. 8f). These results suggested that CCl_4 can promote autophagy and that YQRG treatment inhibits this process.

Effects of YQRG treatment on cell signalling pathways

To further evaluate the mechanism associated with YQRG treatment of liver fibrosis, we evaluated markers related to the pathways identified by KEGG analysis. Western blot analysis of liver tissue samples from the control, model, and YQRG-H groups identified the expression of p38, p-p38, AMPK, and p-AMPK, with upregulated levels of p-p38 and downregulated levels of AMPK and p-AMPK observed in the model group relative to the control group. Following YQRG-H treatment, we found significantly decreased p-p38 levels and increased levels of AMPK and p-AMPK relative to those in the model group (Fig. 9a and b). Moreover, qPCR results were consistent with those of western blot analysis (Fig. 9c and d). These results suggested that YQRG-H treatment inhibiting p38-MAPK signalling and activated AMPK signalling.

Discussion

Hepatic fibrosis is a repair response to chronic liver injury. Due to the proliferation of myofibroblasts under the action of different stimuli, hepatocytes initiate the production of various chemokines, which promote myofibroblast proliferation in the liver injury area and result in the formation of collagen and other fibre components, ECM accumulation, and fibrosis. Liver injury from various causes leads to liver fibrosis, with this potentially followed by cirrhosis and liver cancer. There is currently a lack of therapeutic options for preventing hepatic fibrosis, making it necessary to research and actively develop effective

drugs. YQRG is a traditional Chinese medicine comprised of eight herbs and a mixture of compounds. In this study, we identified YQRG compounds by UHPLC-QTOF-MS, most of which were previously identified as playing a role in improving liver fibrosis
(i.e., *Paeoniflorin, Bisdemethoxycurcumin, Curcumin, Cryptotanshinone, Gallic acid, Protocatechualdehyde, Rosmarinic acid, Salvianolic acid A*) [30-37] (Fig. 1c). This result suggests that most of the sampled compounds may be the components of YQRGs which mitigate against liver fibrosis.

The liver can be damaged by infection, excessive drinking or other stimuli [38], and various liver injuries can promote the expression of fibrogenic mediators and their receptors in response to liver fibrosis [39]. Because CCl_4 exerts hepatotoxicity, its administration can seriously damage hepatocytes [40]. Liver injury is reversible upon removal of the stimuli [41];therefore, numerous studies have evaluated the mechanisms associated with CCl_4-induced liver injury. In this study, we evaluated the effect of YQRG on rat models of CCl_4-induced liver injury and observed significant decreases in weight(Fig. 2a). and increases in the LW:BW ratio (Fig. 2b). in the CCl_4-induced model rats, while weight increased and LW:BW decrease in the YQRG-H group. Moreover, we measured serum ALT and AST levels (Fig. 2c and d) as markers of hepatocyte integrity [42], finding significantly increased levels of both in the model group, whereas these levels were restored to those similar to controls following YQRG treatment. Additionally, H&E staining and TEM analysis (Fig. 2e) identified evidence of pathological hepatocyte injury in the model group; however, these characteristics were significantly improved following YQRG treatment. These results indicate that YQRG treatment effectively Reduced CCl_4-induced liver injury.

YQRG has been used to clinically treat liver fibrosis with good effect; however, there is currently a lack of experimental data supporting its efficacy. Here, we established a rat model of liver fibrosis to evaluate the efficacy and mechanism of YQRG against liver fibrosis induced by CCl_4 [43]. Masson staining (Fig. 3a) to evaluate liver fibrosis revealed fibrous septum in the model group, whereas the YQRG-treated group demonstrated significantly reduced fibrosis. Additionally, we evaluated serum levels of the fibrotic markers HA, LN, PC-III, and IV-C [44]. Hyp, an important component of collagen tissue, comprises up to 13% of collagen [45] and represents another marker of liver fibrosis [46]. In the present study, levels of serum HA, LN, PC-III, IV-C (Fig. 3c) and Hyp (Fig. 3d) in liver tissue in the model group were significantly higher than those in the control and YQRG-treatment groups. Moreover, in liver fibrosis, excessive accumulation of ECM is mainly due to HSC activation [47], we observed significant increases in α-SMA (a marker of HSCs activation [26]) levels detected by IHC (Fig. 3a), Western blot (Fig. 3d) and qPCR (Fig. 3f) in the model group, while decreased after YQRG-H treatment. ECM is regulated by TIMPs and MMPs [24]. A previous study reported that inhibiting HSC activity can reduce TIMPs secretion and increase MMPs activity to promote ECM degradation [48]. Consistent with these findings, in the present study, we found that YQRG-H treatment significantly reduced *Timp1* expression and increased *Mmp9* expression in the model group (Fig. 3g and h). These findings suggested that YQRG treatment effectively improved CCl_4-induced liver fibrosis in rats by attenuating HSCs activity and inhibiting ECM synthesis.

ER is the largest organelle in HPCs and has the functions of participating in protein folding and regulating calcium homeostasis [49,50]. The increased membrane hardness of ER leads to the damage of ER membrane energy, promotes the accumulation of misfolded proteins, and then activates the unfolded protein response (UPR) [51,52]. ATF6, IRE1 and PERK are transmembrane sensors of UPR [53]. ERS is closely related to the increased expression of UPR related genes. For example, Zhan et al. (2020) found that microcystin LR can up-regulate the gene levels of perk and IRE1 in the liver and ovary, causing ERS [54]. In this study, ELISA and mRNA expression levels of liver ATF6, IRE1 and PERK increased after CCl4 treatment (Fig. 5c-e and 5h-j). Under stress-free conditions, BiP, an important member of the heat shock protein 70 family, binds to URP. Under ERS, BiP binds to wrong or unfolded proteins and separates from URP, activates these sensors and their downstream signal cascade through dimerization and autophosphorylation, and promotes the increase of apoptosis regulator CHOP [55]. In our experiment, the ELISA and transcriptional gene levels of BiP and apoptotic transcription factor CHOP in the liver of rats with hepatic fibrosis were higher than those in the YQRG-H group (Fig. 5b and f, 5g and k). Studies have shown that inhibiting ERS can reduce liver fibrosis [56]. In this study, transcriptome analysis showed that ERS inhibition was an important mechanism of YQRG mediated reduction of CCl4 induced liver fibrosis (Fig. 5b and d). This is consistent with our experimental data and transcriptome results, suggesting that YQRG treatment reduces CCl4 induced liver fibrosis in rats by inhibiting ERS.

HPCs apoptosis is an inflammatory stimulus that promotes HSCs and plays an important role in liver diseases [57,58]. Our data show that a significant increase of TUNEL and α-SMA positive cells can be seen in the liver of rats in the CCl_4 group (Fig. 7b).Under sustained ERS, pro-apoptotic signals are induced by activating several transcription factors [59-61]. CHOP is a key transcription factor related to ERS mediated activation of HPCs apoptosis [62]. Under continuous ERS, the pro-apoptotic factor CHOP inhibits the level of downstream anti-apoptotic protein BCL-2. In addition, Ca^{2+} enters the cytoplasm, m-calpain and procaspase 12 are further cleaved and activated, and the caspase cascade induces apoptosis [63]. Apoptosis mainly includes endogenous and exogenous apoptosis. In the endogenous apoptosis pathway, mitochondrial permeability releases cytochrome c, Caspase 9 and Caspase 3 are activated in order. In the exogenous apoptotic pathway, Caspase 3 is activated by upstream bound Caspase 8 and by FADD. Death receptors such as trail bind to FADD to further activate downstream Caspase 8 and Caspase 3, and Caspase 3 is the co-executor of the two pathways [64-67]. In this study, we demonstrated the expression of CHOP, BCL2 and Caspase 12 in fibrotic rats (Fig. 7c-e, 6f and k), indicating that apoptosis occurs during the development of fibrosis. These results were combined with the significant increase of ERS related indexes in the model group, suggesting that CCl_4 may induce apoptosis by activating ERS.

Autophagy is a metabolic process in which autophagosomes formed by cell membranes phagocytize organelles and cell fragments for subsequent lysosomal degradation [68]. Studies have shown that ERS mediated HSCs autophagy promotes the occurrence of liver fibrosis. For example, men R et al. Found that after NOGO-B gene knockout, the levels of ERS and autophagy markers were down-regulated, and the autophagy level could be regulated byERS agonists and antagonists. The results showed that inhibiting

ERS could reduce the autophagy of HSCs [69]. Overexpression of *Ulk1* kinase death mutant can inhibit autophagy [29], and LC3-II represents autophagy marker [28]. Consistently, we found that prolonged exposure to CCl_4 increased the expression of two key autophagy genes (LC3 and ULK1). In this study, LC3-II and α-SMA positive cells increased significantly (Fig. 8b), indicating that the increased autophagy in the liver fibrosis model is related to HSCs activation. The protein and mRNA levels of LC3II increased in the model group and the mRNA expression of *Ulk1* decreased in the model group (Fig. 8c-f). This result well supports our conclusion. In conclusion, these results suggest that YQRG improves liver fibrosis by inhibiting autophagy.

Pathway analysis suggested that YQRG treatment altered the MAPK and AMPK signalling pathways. p38 MAPK plays an important role in regulating inflammation, apoptosis, and liver fibrosis [70,71] and a previous study reported that ERS activates p38 MAPK signalling [72]. Additionally, ERS-mediated IRE1/p38 MAPK signalling promotes the activation of isolated HSCs in rats [73]. In the present study, we found that YQRG treatment inhibited p38 MAPK signalling (Fig. 9a and d) along with the expression of ERS-related markers, suggesting that YQRG might alleviate liver fibrosis by inhibiting ERS through regulation of p38 MAPK signalling. Moreover, p38 MAPK promotes apoptosis [74] and is associated with autophagy induction. AMPK is an energy sensor that plays an important role in maintaining energy homeostasis [75]. A previous study showed that AMPK exerts an anti-apoptotic effect and can inhibit HPC apoptosis [76]. Additionally, AMPK activation inhibited autophagy in an HSC line (lx-2) [77]. In the present study, YQRG treatment promotes AMPK signalling (Fig. 9a and d). Moreover, the observed regulation of apoptosis by YQRG suggests that activation of the AMPK pathway might inhibit apoptosis and autophagy, thereby alleviating the progression of liver fibrosis. However, the precise role of YQRG as a therapeutic agent for liver fibrosis requires further investigation.

Conclusion

In conclusion, combined with transcriptome analysis and experimental verification, YQRG can inhibit CCl_4-induced liver fibrosis through a variety of mechanisms. This study showed that YQRG improved liver pathological injury and function inhibited HSC activity, and reduced ECM accumulation in rats with liver fibrosis. This anti-liver fibrosis effect might be related to the inhibition of ERS, apoptosis and autophagy and the regulation of p38 MAPK and AMPK pathways.

Abbreviations

α-SMA, α-smooth muscle actin; ALT, alanine aminotransferase; AMPK, AMP-activated protein kinase; AST, aspartate aminotransferase; ATF6, activated transcription factor 6; BCL-2, B-cell lymphoma 2; BiP, immunoglobin-binding protein; BSA, bovine serum albumin; CASP12, caspase 12; CCl_4, carbon tetrachloride; CHOP, C/EBP homologous protein; DAPI, 4',6-diamino-2-phenylindole; DEG, differentially-expressed gene; ECM, extracellular matrix; ELISA, enzyme-linked immunosorbent assay; ERS, endoplasmic reticulum stress; GO, Gene Ontology; H&E, haematoxylin and eosin; HA, hemagglutinin; HPCs, hepatic parenchymal cells; HSCs, hepatic stellate cells; HYP, hydroxyproline; IFC,

immunofluorescence; IHC, immunohistochemistry; i.p., intraperitoneal; IRE1, inositolase 1; IV-C , type IV collagen; KEGG, Kyoto Encyclopedia of Genes and Genomes; LN, laminin; LC, light chain; LW:BW, liver-to-body weight ratio; MAPK, mitogen-activated protein kinase; MMP9, matrix metalloproteinase 9; PBS, phosphate-buffered saline; PC-III, procollagen III; PERK, protein kinase R-like ER kinase; PI3K/AKT, phosphoinositide 3-kinase/Akt; PPAR , peroxisome proliferator-activated receptors; PPI, protein–protein interaction; qPCR, quantitative PCR; RNA-seq, RNA sequencing; TBST, Tris-buffered saline with Tween-20; TEM, transmission electron microscopy; TIMP1, tissue inhibitor of metalloproteinase 1; TUNEL, terminal deoxynucleotidyl transferase dUTP nick end labelling; UHPLC- QTOF-MS, ultra-high performance liquid chromatography with quadrupole time-of-flight mass spectrometry; ULK1, unc-51-like autophagy-activating kinase 1; UPR, unfolded protein response; YQRG, Yiqi Rougan decoction

Declarations

Acknowledgements

The authors thank the National Natural Science Foundation of China for its financial support. We would like to thank Editage(www.editage.cn) for English language editing.

Authors' contributions

YX and W-FC conceived and designed this research. YX performed experiments, data analysis, and wrote the manuscript. J-YH, J-YT and CX assisted in the experiments and provided data, K-YT, YL,J-XC and L-YZ assisted in data analysis. Z-YC, X-QD revised the manuscript, W-FC supervised the experiments. All authors have reviewed and approved the final version of the manuscript.

Funding

This research was supported by the National NaturalScience Foundation of China (No. 81573860). The funding body did not participate in the design of the study, collection, analysis, interpretation of data, or in writing the manuscript.

Availability of data and materials

The data used and/or investigated during the present study are available from the corresponding author upon reasonable request.

Ethics approval and consent to participate

The animal study was reviewed and approved by the Ethics Committee of Chongqing Medical University (2021034).

Consent for publication

Not applicable.

Competing interests

The authors have declared no conflict of interest.

References

1. Elpek GÖ. Cellular and molecular mechanisms in the pathogenesis of liver fibrosis: An update. World J Gastroenterol. 2014;20(23):7260-76.
2. Campana L, Iredale JP. Regression of Liver Fibrosis. Semin Liver Dis. 2017;37(1):1-10.
3. Bataller R, Brenner DA. Liver fibrosis. J Clin Invest. 2005;115(2):209-18.
4. Asrani SK, Devarbhavi H, Eaton J, Kamath PS. Burden of liver diseases in the world. J Hepatol. 2019;70(1):151-171.
5. Harris R, Harman DJ, Card TR, Aithal GP, Guha IN. Prevalence of clinically significant liver disease within the general population, as defined by non-invasive markers of liver fibrosis: a systematic review. Lancet Gastroenterol Hepatol. 2017;2(4):288-297.
6. Caballería L, Pera G, Arteaga I, Rodríguez L, Alumà A, Morillas RM, de la Ossa N, Díaz A, Expósito C, Miranda D, et al. High Prevalence of Liver Fibrosis Among European Adults With Unknown Liver Disease: A Population-Based Study. Clin Gastroenterol Hepatol. 2018;16(7):1138-1145.e5.
7. Dong S, Su SB. Advances in mesenchymal stem cells combined with traditional Chinese medicine therapy for liver fibrosis. J Integr Med. 2014;12(3):147-55.
8. Iwaisako K, Jiang C, Zhang M, Cong M, Moore-Morris TJ, Park TJ, Liu X, Xu J, Wang P, Paik YH, et al. Origin of myofibroblasts in the fibrotic liver in mice. Proc Natl Acad Sci U S A. 2014;111(32):E3297-305.
9. Mederacke I, Hsu CC, Troeger JS, Huebener P, Mu X, Dapito DH, Pradere JP, Schwabe RF. Fate tracing reveals hepatic stellate cells as dominant contributors to liver fibrosis independent of its aetiology. Nat Commun. 2013;4:2823.
10. Reeves HL, Friedman SL. Activation of hepatic stellate cells–a key issue in liver fibrosis. Front Biosci. 2002;7:d808-26.
11. Walter P, Ron D. The unfolded protein response: from stress pathway to homeostatic regulation. Science. 2011;334(6059):1081-6.
12. Li X, Wang Y, Wang H, Huang C, Huang Y, Li J. Endoplasmic reticulum stress is the crossroads of autophagy, inflammation, and apoptosis signaling pathways and participates in liver fibrosis. Inflamm Res. 2015;64(1):1-7.
13. Malhi H, Kaufman RJ. Endoplasmic reticulum stress in liver disease. J Hepatol. 2011;54(4):795-809.
14. Seki E, Schwabe RF. Hepatic inflammation and fibrosis: functional links and key pathways. Hepatology. 2015;61(3):1066-79.
15. Brenner C, Galluzzi L, Kepp O, Kroemer G. Decoding cell death signals in liver inflammation. J Hepatol. 2013;59(3):583-94.

16. Lee BH, Hsu WH, Hsu YW, Pan TM. Suppression of dimerumic acid on hepatic fibrosis caused from carboxymethyl-lysine (CML) by attenuating oxidative stress depends on Nrf2 activation in hepatic stellate cells (HSCs). Food Chem Toxicol. 2013;62:413-9.
17. Hernández-Gea V, Friedman SL. Autophagy fuels tissue fibrogenesis. Autophagy. 2012;8(5):849-50.
18. Parzych KR, Klionsky DJ. An overview of autophagy: morphology, mechanism, and regulation. Antioxid Redox Signal. 2014;20(3):460-73.

19 Eom YW, Shim KY, Baik SK. Mesenchymal stem cell therapy for liver fibrosis. Korean J Intern Med. 2015;30(5):580-9.

20 Zhao CQ, Zhou Y, Ping J, Xu LM. Traditional Chinese medicine for treatment of liver diseases: progress, challenges and opportunities. J Integr Med. 2014;12(5):401-8.

21 Wang Z, Gerstein M, Snyder M. RNA-Seq: a revolutionary tool for transcriptomics. Nat Rev Genet. 2009;10(1):57-63.

22 Chen X, Long L, Cheng Y, Chu J, Shen Z, Liu L, Li J, Xie Q, Liu H, Wu M, Chen Y, Peng J, Shen A. Qingda granule attenuates cardiac fibrosis via suppression of the TGF-β1/Smad2/3 signaling pathway in vitro and in vivo. Biomed Pharmacother. 2021;137:111318.

23 Zhou Y, Wu R, Cai FF, Zhou WJ, Lu YY, Zhang H, Chen QL, Su SB. Xiaoyaosan decoction alleviated rat liver fibrosis via the TGFβ/Smad and Akt/FoxO3 signaling pathways based on network pharmacology analysis. J Ethnopharmacol. 2021;264:113021.

24 Tsuchida T, Friedman SL. Mechanisms of hepatic stellate cell activation. Nat Rev Gastroenterol Hepatol. 2017;14(7):397-411.

25 Xia SW, Wang ZM, Sun SM, Su Y, Li ZH, Shao JJ, Tan SZ, Chen AP, Wang SJ, Zhang ZL, et al. Endoplasmic reticulum stress and protein degradation in chronic liver disease. Pharmacol Res. 2020;161:105218.

26 Puche JE, Saiman Y, Friedman SL. Hepatic stellate cells and liver fibrosis. Compr Physiol. 2013;3(4):1473-92.

27 Paridaens A, Raevens S, Devisscher L, Bogaerts E, Verhelst X, Hoorens A, Van Vlierberghe H, van Grunsven LA, Geerts A, Colle I. Modulation of the Unfolded Protein Response by Tauroursodeoxycholic Acid Counteracts Apoptotic Cell Death and Fibrosis in a Mouse Model for Secondary Biliary Liver Fibrosis. Int J Mol Sci. 2017;18(1):214.

28 Ichimura Y, Kirisako T, Takao T, Satomi Y, Shimonishi Y, Ishihara N, Mizushima N, Tanida I, Kominami E, Ohsumi M, Noda T, Ohsumi Y. A ubiquitin-like system mediates protein lipidation. Nature. 2000;408(6811):488-92.

29Jung CH, Jun CB, Ro SH, Kim YM, Otto NM, Cao J, Kundu M, Kim DH. ULK-Atg13-FIP200 complexes mediate mTOR signaling to the autophagy machinery. Mol Biol Cell. 2009;20(7):1992-2003.

30Ma X, Zhang W, Jiang Y, Wen J, Wei S, Zhao Y. Paeoniflorin, a Natural Product With Multiple Targets in Liver Diseases-A Mini Review. Front Pharmacol. 2020;11:531.

31Lee PJ, Woo SJ, Jee JG, Sung SH, Kim HP. Bisdemethoxycurcumin Induces apoptosis in activated hepatic stellate cells via cannabinoid receptor 2. Molecules. 2015;20(1):1277-92.

32Kong D, Zhang Z, Chen L, Huang W, Zhang F, Wang L, Wang Y, Cao P, Zheng S. Curcumin blunts epithelial-mesenchymal transition of hepatocytes to alleviate hepatic fibrosis through regulating oxidative stress and autophagy. Redox Biol. 2020;36:101600.

33Nagappan A, Kim JH, Jung DY, Jung MH. Cryptotanshinone from the *Salvia miltiorrhiza* Bunge Attenuates Ethanol-Induced Liver Injury by Activation of AMPK/SIRT1 and Nrf2 Signaling Pathways. Int J Mol Sci. 2019;21(1):265.

34Chen Y, Zhou Z, Mo Q, Zhou G, Wang Y. Gallic Acid Attenuates Dimethylnitrosamine-Induced Liver Fibrosis by Alteration of Smad Phosphoisoform Signaling in Rats. Biomed Res Int. 2018;2018:1682743.

35Lv T, Yao XX. Comparison of protocatechuic aldchyde in Radix Salvia miltiorrhiza and corresponding pharmacological sera from normal and fibrotic rats by high performance liquid chromatography. World J Gastroenterol. 2006;12(14):2195-200.

36Li GS, Jiang WL, Tian JW, Qu GW, Zhu HB, Fu FH. In vitro and in vivo antifibrotic effects of rosmarinic acid on experimental liver fibrosis. Phytomedicine. 2010;17(3-4):282-8.

37Zhu J, Wang R, Xu T, Zhang S, Zhao Y, Li Z, Wang C, Zhou J, Gao D, Hu Y, Tian X, Yao J. Salvianolic Acid A Attenuates Endoplasmic Reticulum Stress and Protects Against Cholestasis-Induced Liver Fibrosis via the SIRT1/HSF1 Pathway. Front Pharmacol. 2018;9:1277.

38Rutherford A, Chung RT. Acute liver failure: mechanisms of hepatocyte injury and regeneration. Semin Liver Dis. 2008;28(2):167-74.

39Toosi AE. Liver Fibrosis: Causes and Methods of Assessment, A Review. Rom J Intern Med. 2015;53(4):304-14.

40Kanta J, Dooley S, Delvoux B, Breuer S, D'Amico T, Gressner AM. Tropoelastin expression is up-regulated during activation of hepatic stellate cells and in the livers of CCl(4)-cirrhotic rats. Liver. 2002;22(3):220-7.

41Atta HM. Reversibility and heritability of liver fibrosis: Implications for research and therapy. World J Gastroenterol. 2015;21(17):5138-48.

42 Fallatah HI, Akbar HO, Fallatah AM. Fibroscan Compared to FIB-4, APRI, and AST/ALT Ratio for Assessment of Liver Fibrosis in Saudi Patients With Nonalcoholic Fatty Liver Disease. Hepat Mon. 2016;16(7):e38346.

43 Abdel-Moneim AM, Al-Kahtani MA, El-Kersh MA, Al-Omair MA. Free Radical-Scavenging, Anti-Inflammatory/Anti-Fibrotic and Hepatoprotective Actions of Taurine and Silymarin against CCl4 Induced Rat Liver Damage. PLoS One. 2015;10(12):e0144509.

44 LLou X, Hou Y, Cao H, Zhao J, Zhu F. Clinical significance of decoy receptor 3 upregulation in patients with hepatitis B and liver fibrosis. Oncol Lett. 2018;16(1):1147-1154.

45 Kim YO, Popov Y, Schuppan D. Optimized Mouse Models for Liver Fibrosis. Methods Mol Biol. 2017;1559:279-296.

46 García L, Hernández I, Sandoval A, Salazar A, Garcia J, Vera J, Grijalva G, Muriel P, Margolin S, Armendariz-Borunda J. Pirfenidone effectively reverses experimental liver fibrosis. J Hepatol. 2002;37(6):797-805.

47 Iwaisako K, Jiang C, Zhang M, Cong M, Moore-Morris TJ, Park TJ, Liu X, Xu J, Wang P, Paik YH, et al. Origin of myofibroblasts in the fibrotic liver in mice. Proc Natl Acad Sci U S A. 2014;111(32):E3297-305.

48 Hemmann S, Graf J, Roderfeld M, Roeb E. Expression of MMPs and TIMPs in liver fibrosis-a systematic review with special emphasis on anti-fibrotic strategies. J Hepatol. 2007;46(5):955-75.

49 Bravo R, Parra V, Gatica D, Rodriguez AE, Torrealba N, Paredes F, Wang ZV, Zorzano A, Hill JA, Jaimovich E, et al. Endoplasmic reticulum and the unfolded protein response: dynamics and metabolic integration. Int Rev Cell Mol Biol. 2013;301:215-90.

50 Sovolyova N, Healy S, Samali A, Logue SE. Stressed to death-mechanisms of ER stress-induced cell death. Biol Chem. 2014;395(1):1-13.

51 Hager L, Li L, Pun H, Liu L, Hossain MA, Maguire GF, Naples M, Baker C, Magomedova L, Tam J, et al. Lecithin:cholesterol acyltransferase deficiency protects against cholesterol-induced hepatic endoplasmic reticulum stress in mice. J Biol Chem. 2012;287(24):20755-68.

52 Hollien J. Evolution of the unfolded protein response. Biochim Biophys Acta. 2013;1833(11):2458-63.

53 Frakes AE, Dillin A. The UPRER: Sensor and Coordinator of Organismal Homeostasis. Mol Cell. 2017;66(6):761-771.

54 Zhan C, Liu W, Zhang F, Zhang X. Microcystin-LR triggers different endoplasmic reticulum stress pathways in the liver, ovary, and offspring of zebrafish (Danio rerio). J Hazard Mater. 2020;386:121939.

55Behnke J, Feige MJ, Hendershot LM. BiP and its nucleotide exchange factors Grp170 and Sil1: mechanisms of action and biological functions. J Mol Biol. 2015;427(7):1589-608.

56Loeuillard E, El Mourabit H, Lei L, Lemoinne S, Housset C, Cadoret A. Endoplasmic reticulum stress induces inverse regulations of major functions in portal myofibroblasts during liver fibrosis progression. Biochim Biophys Acta Mol Basis Dis. 2018;1864(12):3688-3696.

57Liu C, Wang G, Chen G, Mu Y, Zhang L, Hu X, Sun M, Liu C, Liu P. Huangqi decoction inhibits apoptosis and fibrosis, but promotes Kupffer cell activation in dimethylnitrosamine-induced rat liver fibrosis. BMC Complement Altern Med. 2012;12:51.

58Friedman SL. Mechanisms of hepatic fibrogenesis. Gastroenterology. 2008;134(6):1655-69.

59Behnke J, Feige MJ, Hendershot LM. BiP and its nucleotide exchange factors Grp170 and Sil1: mechanisms of action and biological functions. J Mol Biol. 2015;427(7):1589-608.

60Morishima N, Nakanishi K, Takenouchi H, Shibata T, Yasuhiko Y. An endoplasmic reticulum stress-specific caspase cascade in apoptosis. Cytochrome c-independent activation of caspase-9 by caspase-12. J Biol Chem. 2002;277(37):34287-94.

61Xie Q, Khaoustov VI, Chung CC, Sohn J, Krishnan B, Lewis DE, Yoffe B. Effect of tauroursodeoxycholic acid on endoplasmic reticulum stress-induced caspase-12 activation. Hepatology. 2002;36(3):592-601.

62Oyadomari S, Mori M. Roles of CHOP/GADD153 in endoplasmic reticulum stress. Cell Death Differ. 2004;11(4):381-9.

63Wu J, Kaufman RJ. From acute ER stress to physiological roles of the Unfolded Protein Response. Cell Death Differ. 2006;13(3):374-84.

64Liu Y, Yao W, Xu J, Qiu Y, Cao F, Li S, Yang S, Yang H, Wu Z, Hou Y. The anti-inflammatory effects of acetaminophen and N-acetylcysteine through suppression of the NLRP3 inflammasome pathway in LPS-challenged piglet mononuclear phagocytes. Innate Immun. 2015;21(6):587-97.

65Oh SH, Yun KJ, Nan JX, Sohn DH, Lee BH. Changes in expression and immunolocalization of protein associated with toxic bile salts-induced apoptosis in rat hepatocytes. Arch Toxicol. 2003;77(2):110-5.

66Demirbilek S, Tas E, Gurunluoglu K, Akin M, Aksoy RT, Emre MH, Aydin NE, Ay S, Ozatay N. Fluvastatin reduced liver injury in rat model of extrahepatic cholestasis. Pediatr Surg Int. 2007;23(2):155-62.

67. Yang H, Li TW, Ko KS, Xia M, Lu SC. Switch from Mnt-Max to Myc-Max induces p53 and cyclin D1 expression and apoptosis during cholestasis in mouse and human hepatocytes. Hepatology. 2009;49(3):860-70.

68 Dikic I, Elazar Z. Mechanism and medical implications of mammalian autophagy. Nat Rev Mol Cell Biol. 2018;19(6):349-364.

69 Men R, Wen M, Dan X, Zhu Y, Wang W, Li J, Wu W, Liu X, Yang L. Nogo-B: A potential indicator for hepatic cirrhosis and regulator in hepatic stellate cell activation. Hepatol Res. 2015;45(1):113-22.

70 Debacq-Chainiaux F, Boilan E, Dedessus Le Moutier J, Weemaels G, Toussaint O. p38(MAPK) in the senescence of human and murine fibroblasts. Adv Exp Med Biol. 2010;694:126-37.

71 Zhang YP, Yao XX, Zhao X. Interleukin-1 beta up-regulates tissue inhibitor of matrix metalloproteinase-1 mRNA and phosphorylation of c-jun N-terminal kinase and p38 in hepatic stellate cells. World J Gastroenterol. 2006;12(9):1392-6.

72 Hung JH, Su IJ, Lei HY, Wang HC, Lin WC, Chang WT, Huang W, Chang WC, Chang YS, Chen CC, et al. Endoplasmic reticulum stress stimulates the expression of cyclooxygenase-2 through activation of NF-kappaB and pp38 mitogen-activated protein kinase. J Biol Chem. 2004;279(45):46384-92.

73 Hernández-Gea V, Hilscher M, Rozenfeld R, Lim MP, Nieto N, Werner S, Devi LA, Friedman SL. Endoplasmic reticulum stress induces fibrogenic activity in hepatic stellate cells through autophagy. J Hepatol. 2013;59(1):98-104.

74 Wang Y, Wang R, Wang Y, Peng R, Wu Y, Yuan Y. Ginkgo biloba extract mitigates liver fibrosis and apoptosis by regulating p38 MAPK, NF-κB/IκBα, and Bcl-2/Bax signaling. Drug Des Devel Ther. 2015;9:6303-17.

75 Hardie DG. AMP-activated protein kinase: an energy sensor that regulates all aspects of cell function. Genes Dev. 2011;25(18):1895-908.

76 Xie X, Xu X, Sun C, Yu Z. Protective effects of cilostazol on ethanol-induced damage in primary cultured hepatocytes. Cell Stress Chaperones. 2018;23(2):203-211.

77 Kong D, Zhang Z, Chen L, Huang W, Zhang F, Wang L, Wang Y, Cao P, Zheng S. Curcumin blunts epithelial-mesenchymal transition of hepatocytes to alleviate hepatic fibrosis through regulating oxidative stress and autophagy. Redox Biol. 2020;36:101600.

Tables

Table 1 Composition of Yiqi Rougan decoction.

Herbal medicine	Pinyin name	Batch number	herb dose (g)	Occupied Percent (%)
Astragalus mongholicus Bunge	Huang Qi	191210600	30	27.3
Atractylodes Macrocephala Koidz	Bai Zhu	200310099	10	9.1
Salvia miltiorrhizae Bunge	Dan Shen	200201	15	13.6
Curcuma longa L	Jiang Huang	200210064	10	9.1
Paeonia lactiflora Pall	Bai Shao	200210085	15	13.6
Cyperus rotundus L	Xiang Fu	191210613	10	9.1
Sargassum fusiforme Setch	Hai Zao	190701	10	9.1
Trichosanthes Kirilowii Maxim	Gua Lou	190610208	10	9.1

Table 2 Primer sequences used for PCR.

Gene		Oligonucleotide sequence （5’-3’）
Acta2	Forward	AGACACCATGTGTGACGAGG
	Reverse	GACCCATACCGACCATGACA
Mmp9	Forward	CCAACCTTTACCAGCTACTCG
	Reverse	TGAGTTCAATCCCCAGATGCC
Timp1	Forward	CAAAGGATTCGACGCTGTGG
	Reverse	TTCCGTTCCTTAAACGGCCC
Atf6	Forward	CGCCGCAAGAAGAAGGAGTA
	Reverse	CCTTCCTGTTTCCAGACCCC
Ern1	Forward	CGATGGACTGGTGGTAACTG
	Reverse	TGTCTCCTTGGGGAATGGAT
Eif2ak3	Forward	GCTTGCTCCCACATCGGATA
	Reverse	TGCGGCAATTCGTCCATCTA
Hspa5	Forward	AGCCTGGTATGAGGATCTGC
	Reverse	GACTGGAATCTGGAGAGCGA
Chop	Forward	AGCCTGGTATGAGGATCTGC
	Reverse	GACTGGAATCTGGAGAGCGA
Casp12	Forward	AGGCCCATGTGGAGACAGAT
	Reverse	GAGCCACTCTTGCCTACCTT
Bcl2	Forward	CTGGTGGACAACATCGCTCT
	Reverse	GCATGCTGGGGCCATATAGT

Lc3b	Forward	CACAAGGGAAGTGATCGTCG
	Reverse	AGCTGCTTCTCACCCTTGTA
Ulk1	Forward	CATGGTCCCAGCCCAGTTTC
	Reverse	TCGGAGAGGGAGATGGGGTA
P38	Forward	AGATCAAGATCATTGCTCCTCCT
	Reverse	ACGCAGCTCAGTAACAGTCC
Ampk	Forward	AGATCAAGATCATTGCTCCTCCT
	Reverse	ACGCAGCTCAGTAACAGTCC
β-actin	Forward	AGATCAAGATCATTGCTCCTCCT
	Reverse	ACGCAGCTCAGTAACAGTCC

Table 3 The major DEGs and their network degrees

name	degree	name	degree	name	degree
Hspa5	29	*Rab7b*	13	*Bag3*	9
Hsp90aa1	26	*Dnajb9*	12	*Birc3*	9
Jun	24	*Hyou1*	12	*Derl3*	9
Ddit3	23	*Ppp1r15a*	12	*Eif2ak3*	9
Atf4	21	*Bcl2*	11	*HSPA1B*	9
Atf6	19	*Gabarapl2*	11	*Tuba4a*	9
Sqstm1	18	*Hspb11*	11	*Gadd45a*	8
Prkaca	16	*Mapk9*	11	*Lamp2*	8
Apaf1	15	*Ulk1*	11	*Manf*	8
Ern1	14	*App*	10	*Ngf*	8
Irs1	14	*Actg1*	9	*Ulk2*	8

Figures

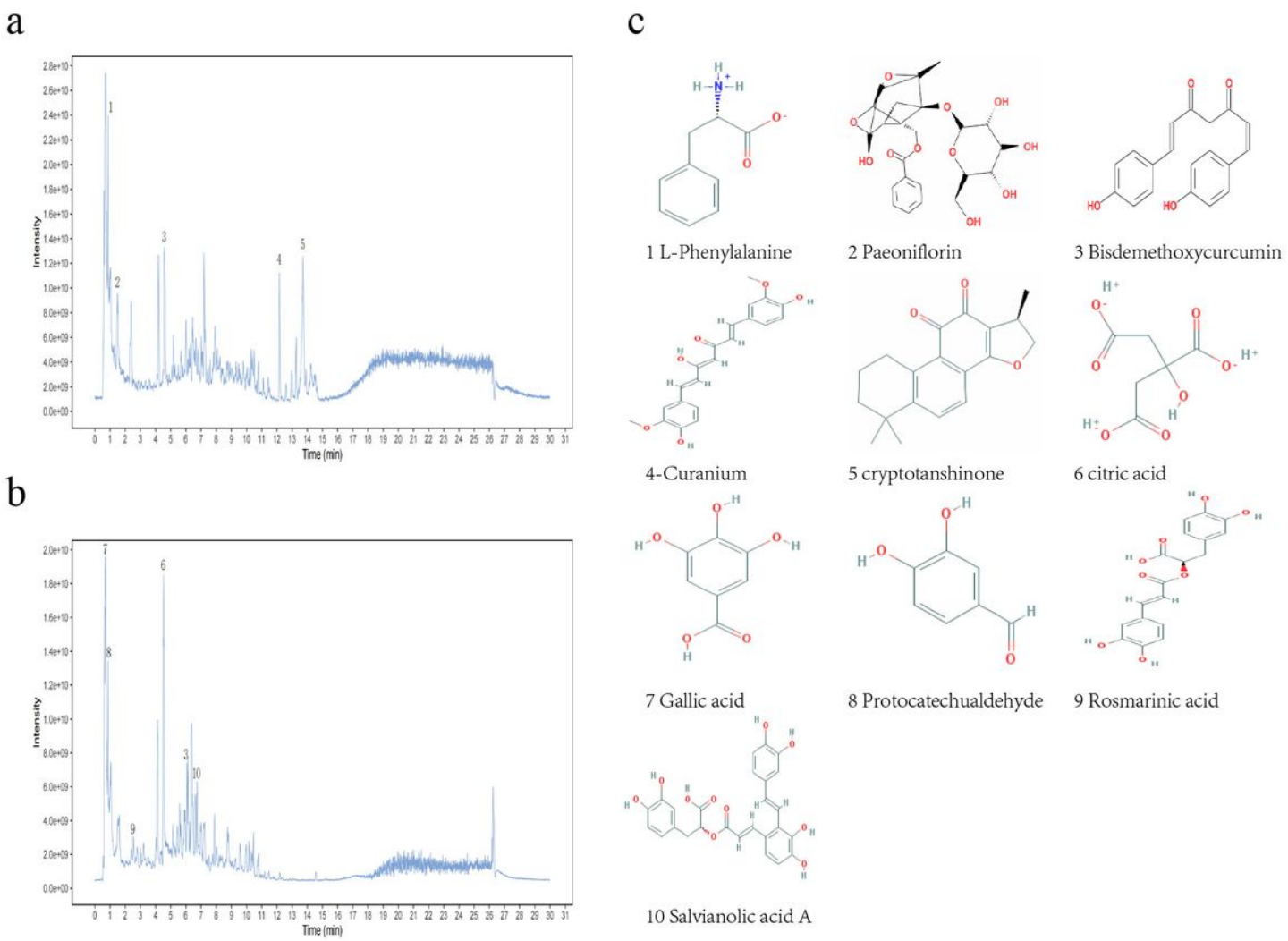

Figure 1

Identification of components of YQRG.Total ion chromatography in positive (a) and negative (b) ion modes for YQRG samples were examined by UHPLC–MS/MS. (c) Molecular structure of constituents

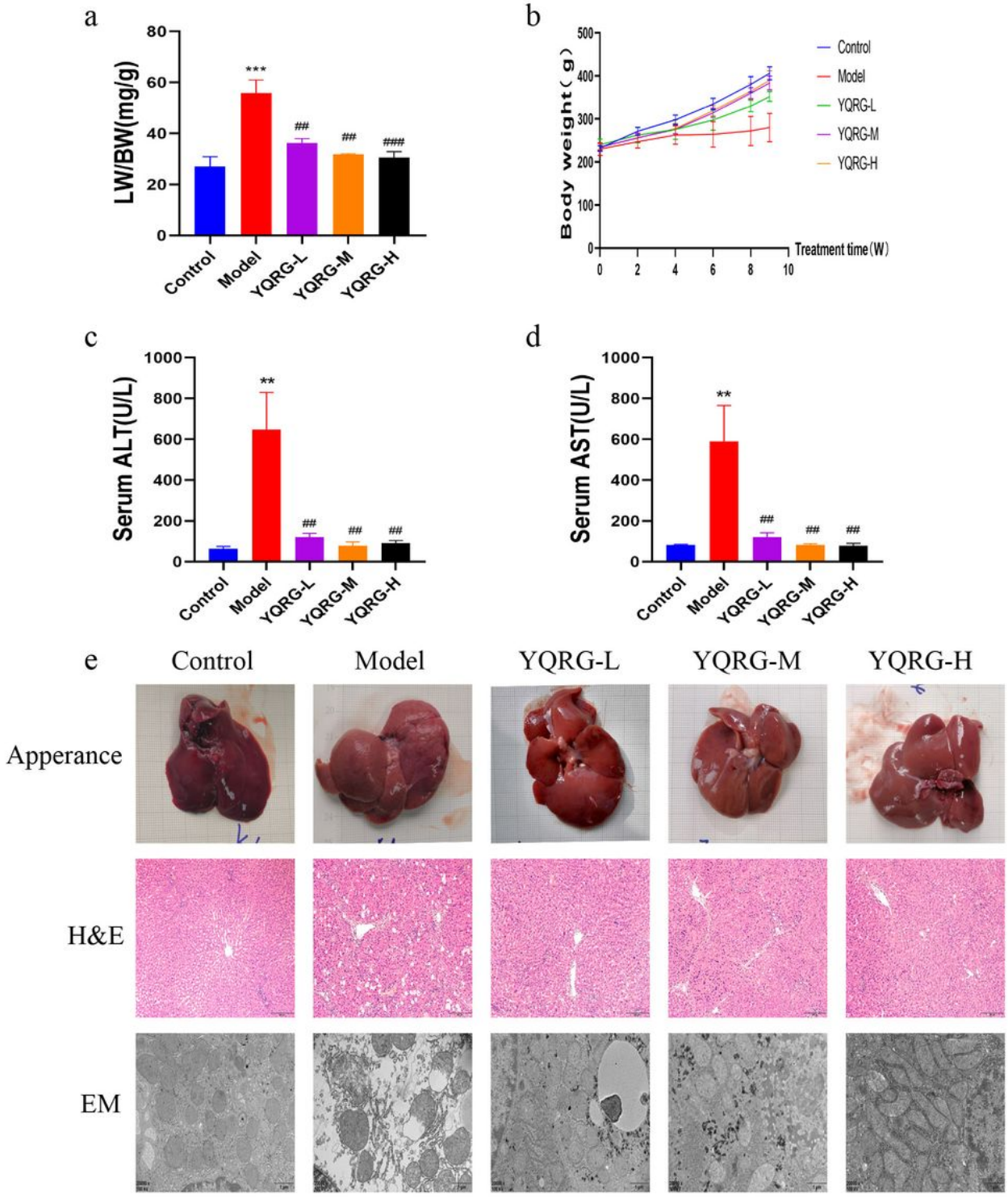

Figure 2

YQRG improves CCl4-induced liver injury in rats. (a) body weight in the different groups. (b) LW/BW ratio in the different groups. (c) and (d) Serum ALT and AST activities. (e) liver pathological changes were analyzed by liver appearance, H&E-staining(100X) of liver sections and transmission electron microscopy of rat livers. Data values were indicated as mean ± SD. *P < 0.05, **P < 0.01 ,***P < 0.001, vs. control group; #P < 0.05, ##P < 0.01, ###P < 0.001, vs. model group

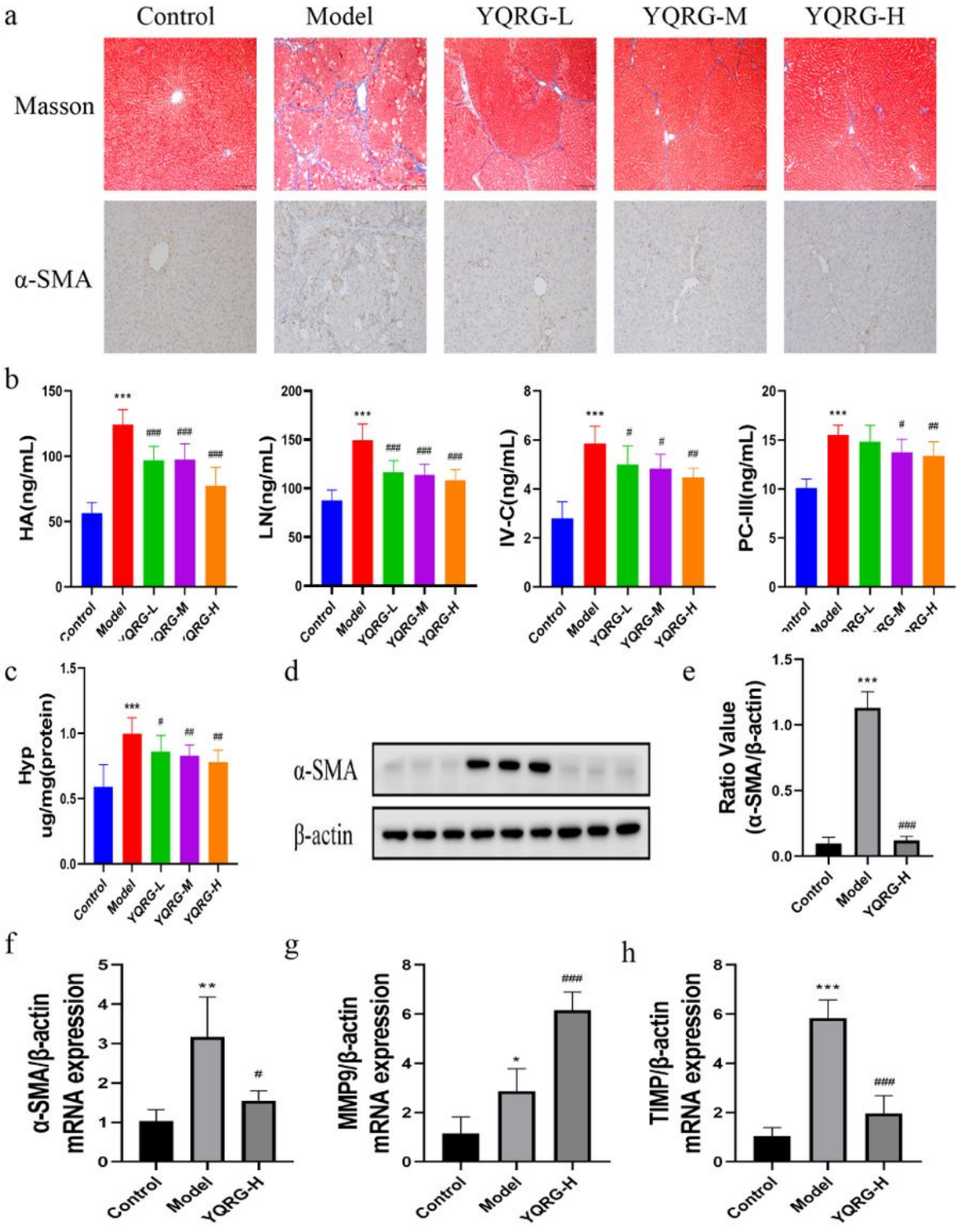

Figure 3

YQRG alleviates CCl4-induced liver fibrosis in rats. (a) Masson staining (100X) of rat livers and α-SMA were detected by immunohistochemistry(200X). (b) Serum HA, LN, PC-III and IV-C content. (c) Hyp contents in liver tissues. (d) Western blot image showing α-SMA expression in liver tissues. (e) Protein concentration analysis. (f-h) mRNA expression of α-SMA, MMP9, TIMP1 were detected by PCR. Data

values were indicated as mean ± SD. *P < 0.05, **P < 0.01 ,***P < 0.001, vs. control group; #P < 0.05, ##P < 0.01, ###P < 0.001, vs. model group

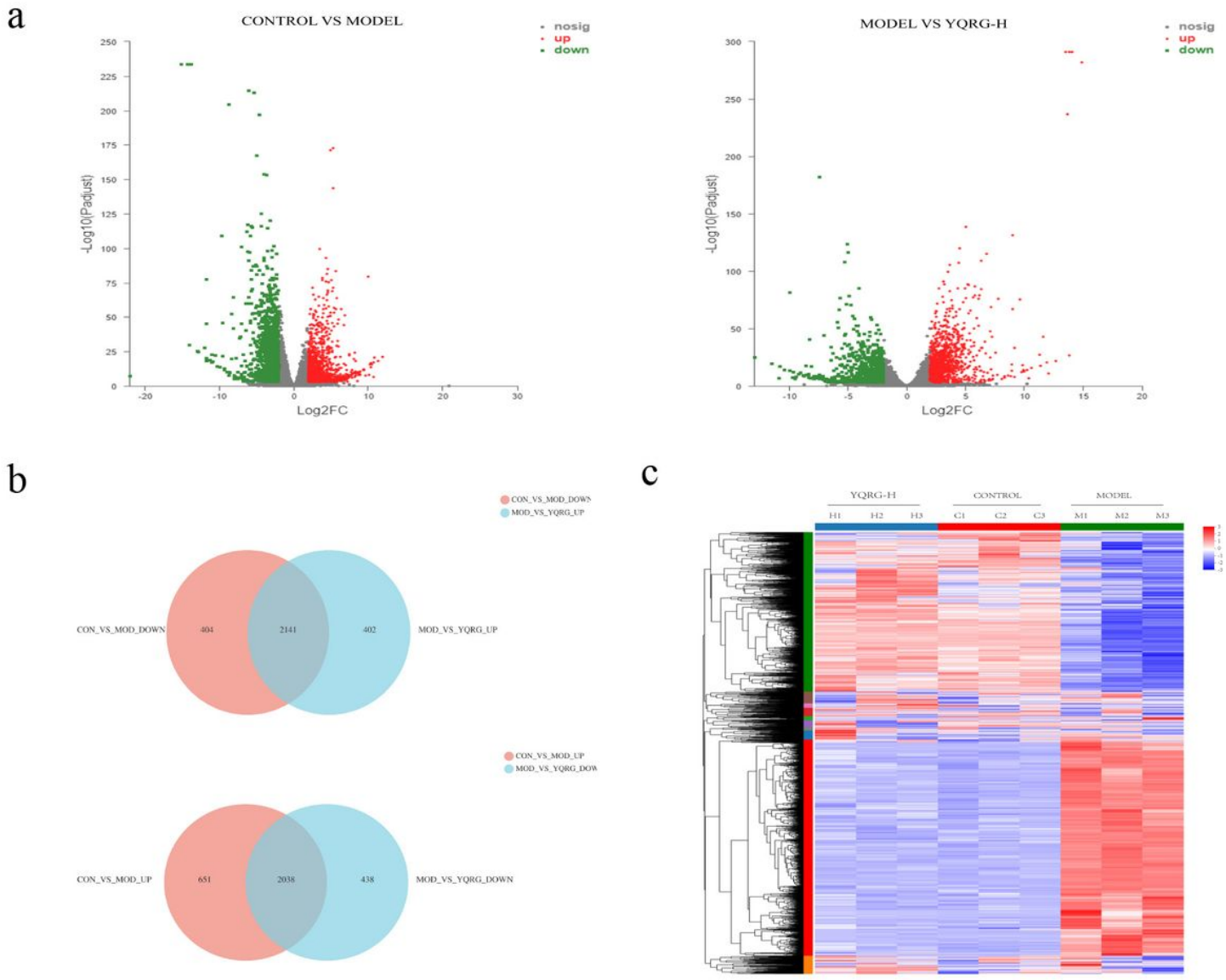

Figure 4

Gene expression analysis by RNA-seq. (a) Volcanic map of upregulated and downregulated DEGs between groups. (b) Venn diagram of the overlap of DEGs between groups. (c) Heat map for hierarchical cluster analysis of DEGs between samples.

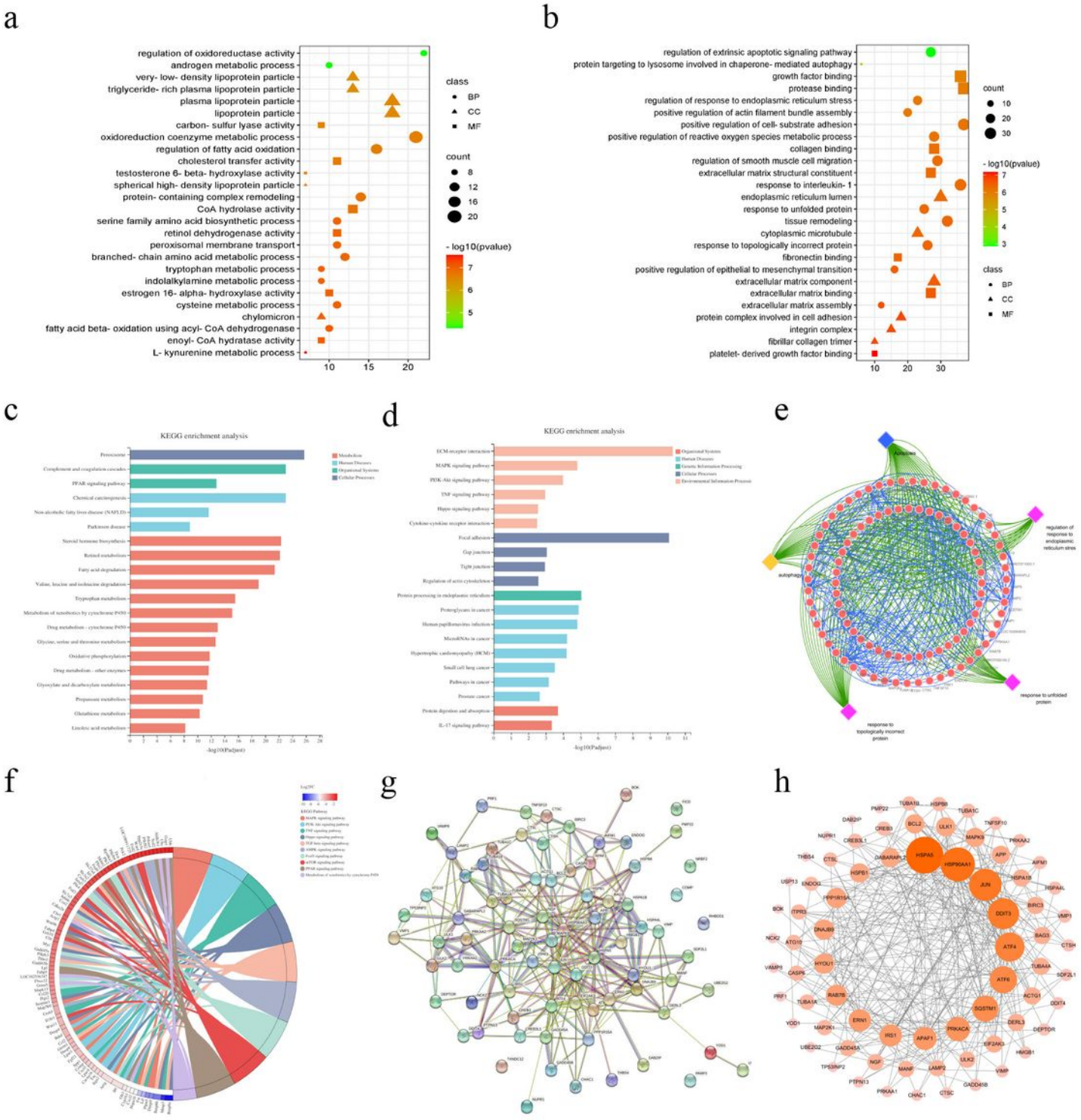

Figure 5

GO, KEGG analysis and PPI network. (a and b) GO enrichment analysis of 2141 overlapping upregulate DEGs and 2038 overlapping downregulate DEGs. (c and d) KEGG enrichment analysis of 2141 overlapping upregulate DEGs and 2038 overlapping downregulates DEGs. (e) Interrelationships between genes involved in ERS, apoptosis, and autophagy. (f) Top 15 major KEGG signalling pathways involved in the anti-fibrosis effect of YQRG. GO results were categorized into three parts: biological (red), cellular

component (green), and molecular function (blue). (g) PPI network of DEGs involved in ERS, apoptosis, and autophagy in the STRING. (h) Visualization of PPI network by the Cytoscape. circular nodes represent the major DEGs of YQRG; The size of these DEGs is positively related to their degrees in the network

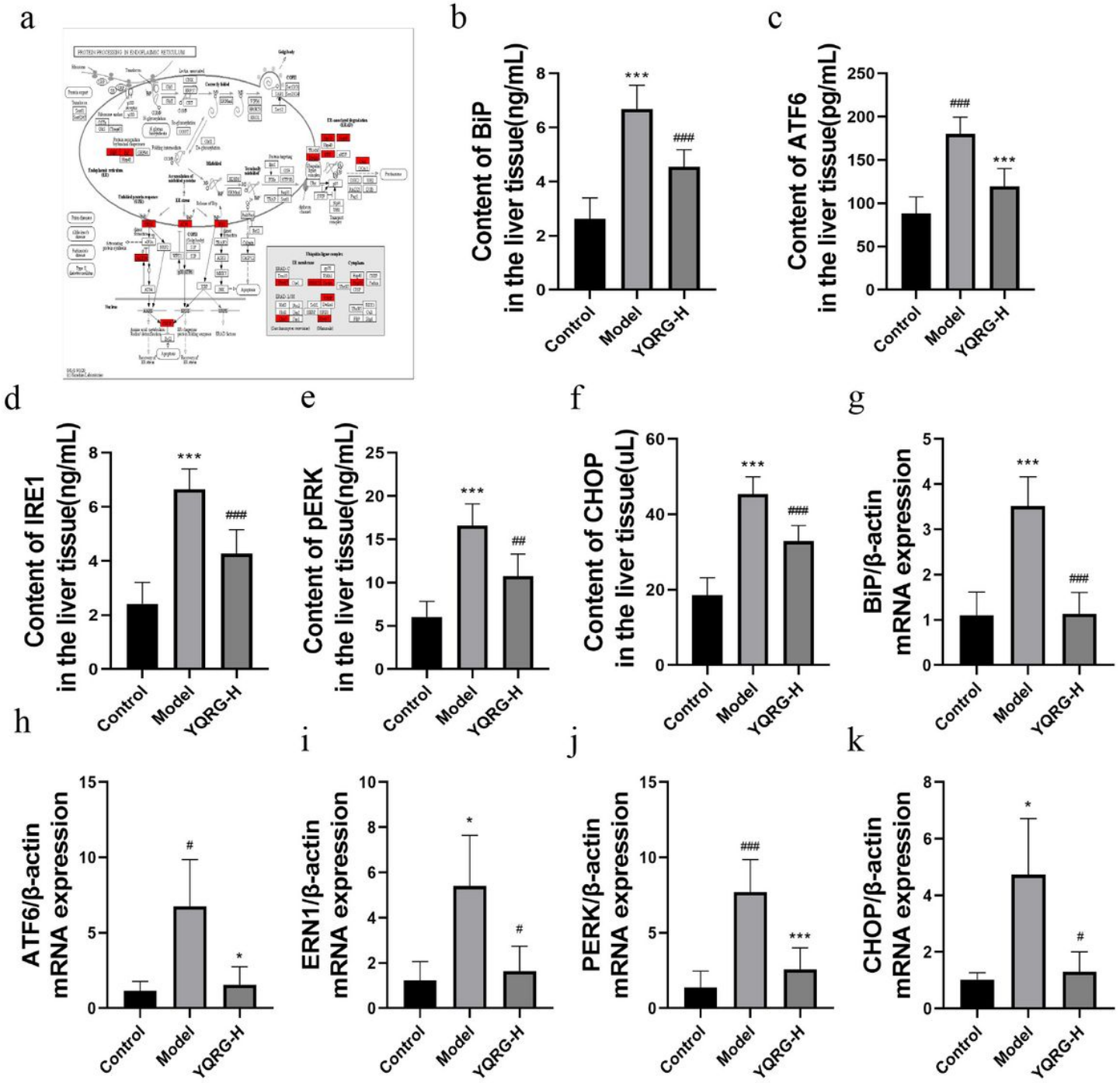

Figure 6

YQRG regulates ERS. (a) Mechanisms of ERS. (b-f) Levels of BiP, ATF6, IRE1, PERK and CHOP were detected by ELISA in liver tissues. (g-k) mRNA expression of BiP, ATF6, ERN1, PERK and CHOP were

detected by PCR. Data values were indicated as mean ± SD. *P < 0.05, **P < 0.01 ,***P < 0.001, vs. control group; #P < 0.05, ##P < 0.01, ###P < 0.001, vs. model group

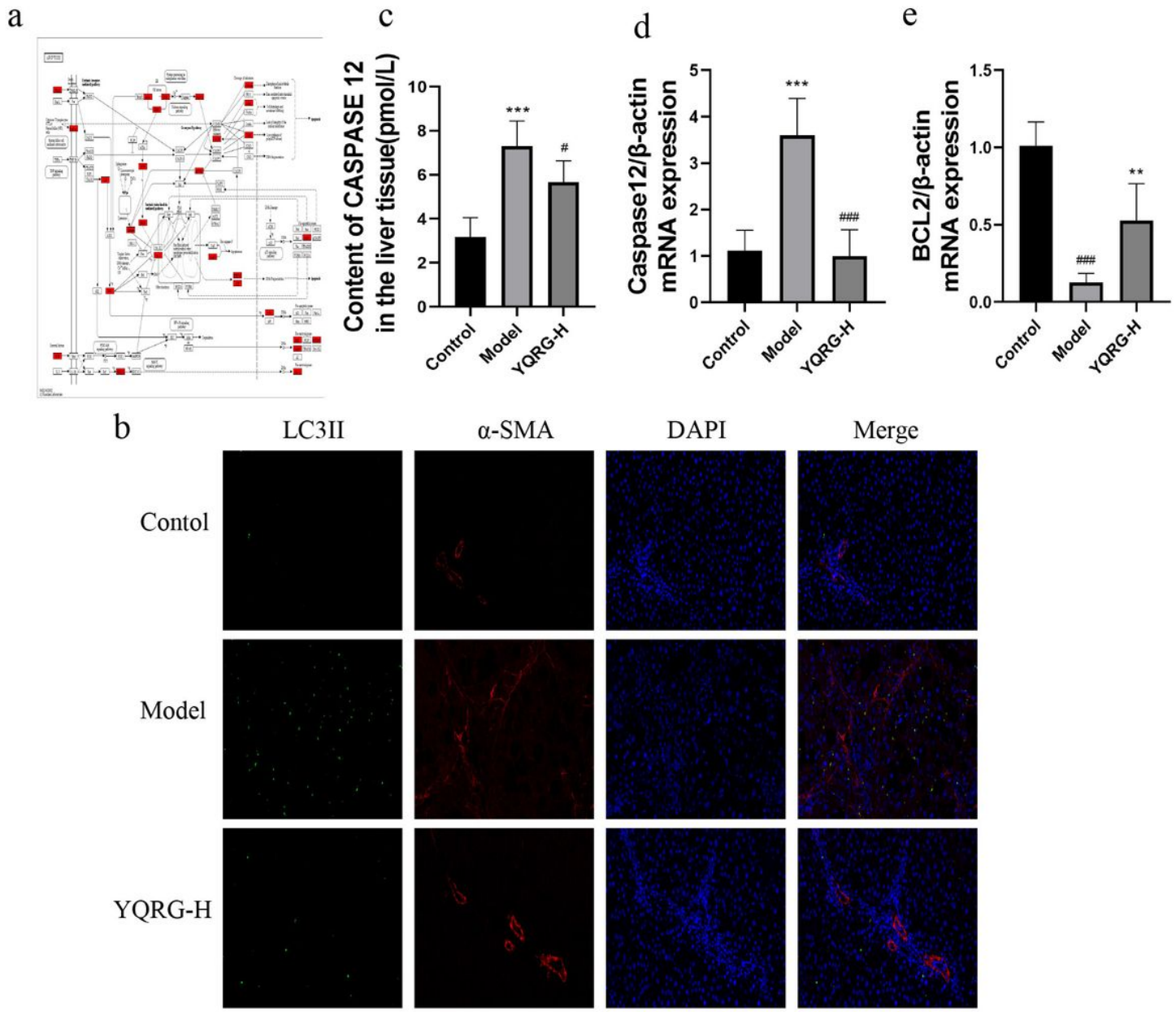

Figure 7

YQRG regulates Apoptosis. (a) Mechanisms of Apoptosis. (b) TUNEL and α-SMA double immunofluorescence staining in liver tissues(Scale bar=50 μm), green fluorescence indicated the Apoptosis cells, red fluorescence represented α-SMA. (c) Levels of Caspase 12 were detected by ELISA in liver tissues.(d-e) mRNA expression of Caspase 12 and Bcl2 were detected by qPCR. Data values were indicated as mean ± SD. *P < 0.05, **P < 0.01 ,***P < 0.001, vs. control group; #P < 0.05, ##P < 0.01, ###P < 0.001, vs. model group

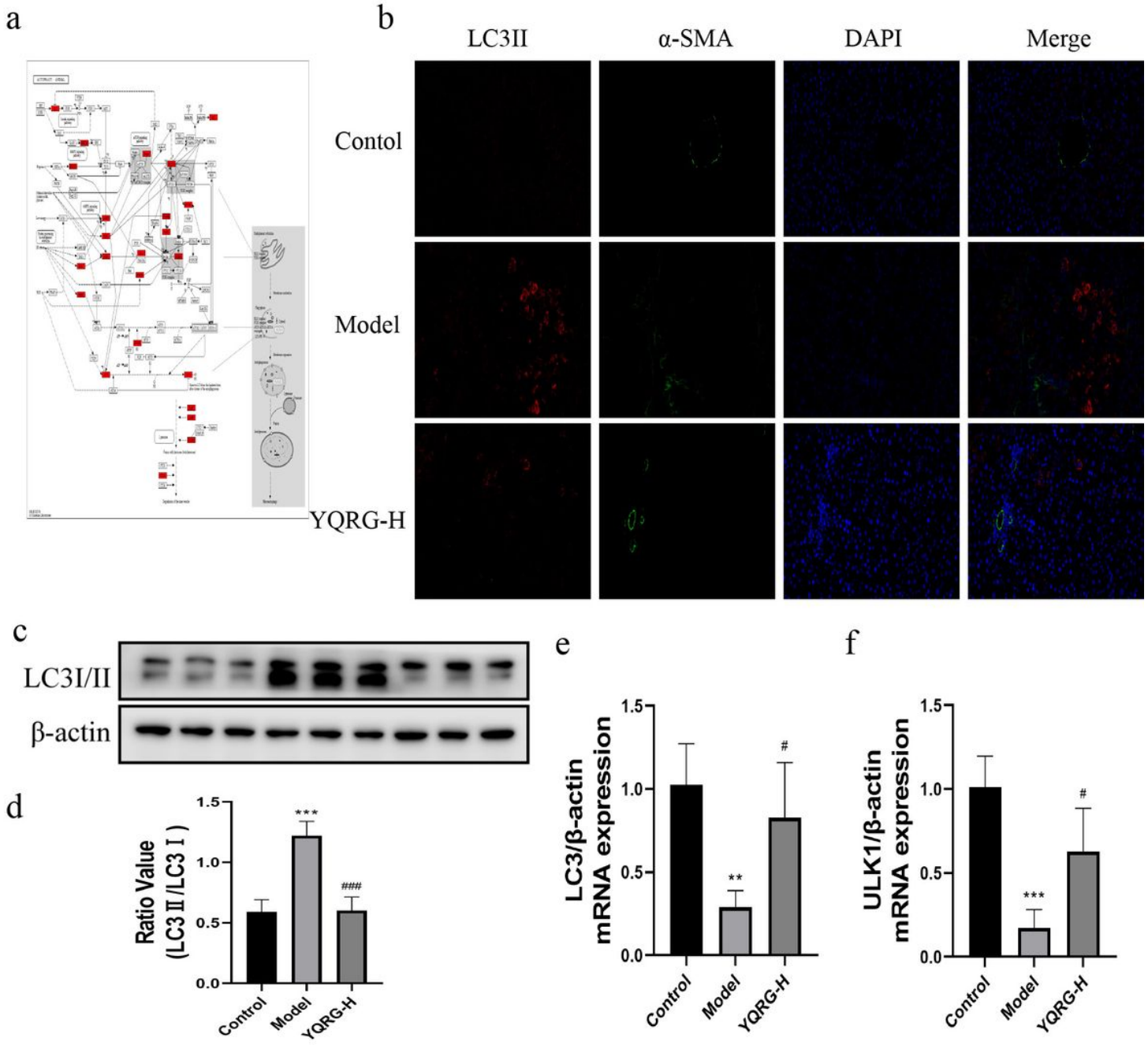

Figure 8

YQRG regulates autophagy. (a) Mechanisms of autophagy. (b) Double immunofluorescent staining was performed to determine the colocalization of LC3II (green) and a-SMA (red) in liver tissues (Scale bar=50 μm). (c) Western blot image showing LC3I/II expression in liver tissues. (d) Protein concentration analysis. (e-f) mRNA expression of LC3II and ULK1 were detected by qPCR. Data values were indicated as mean ± SD. *P < 0.05, **P < 0.01 ,***P < 0.001, vs. control group; #P < 0.05, ##P < 0.01, ###P < 0.001, vs. model group

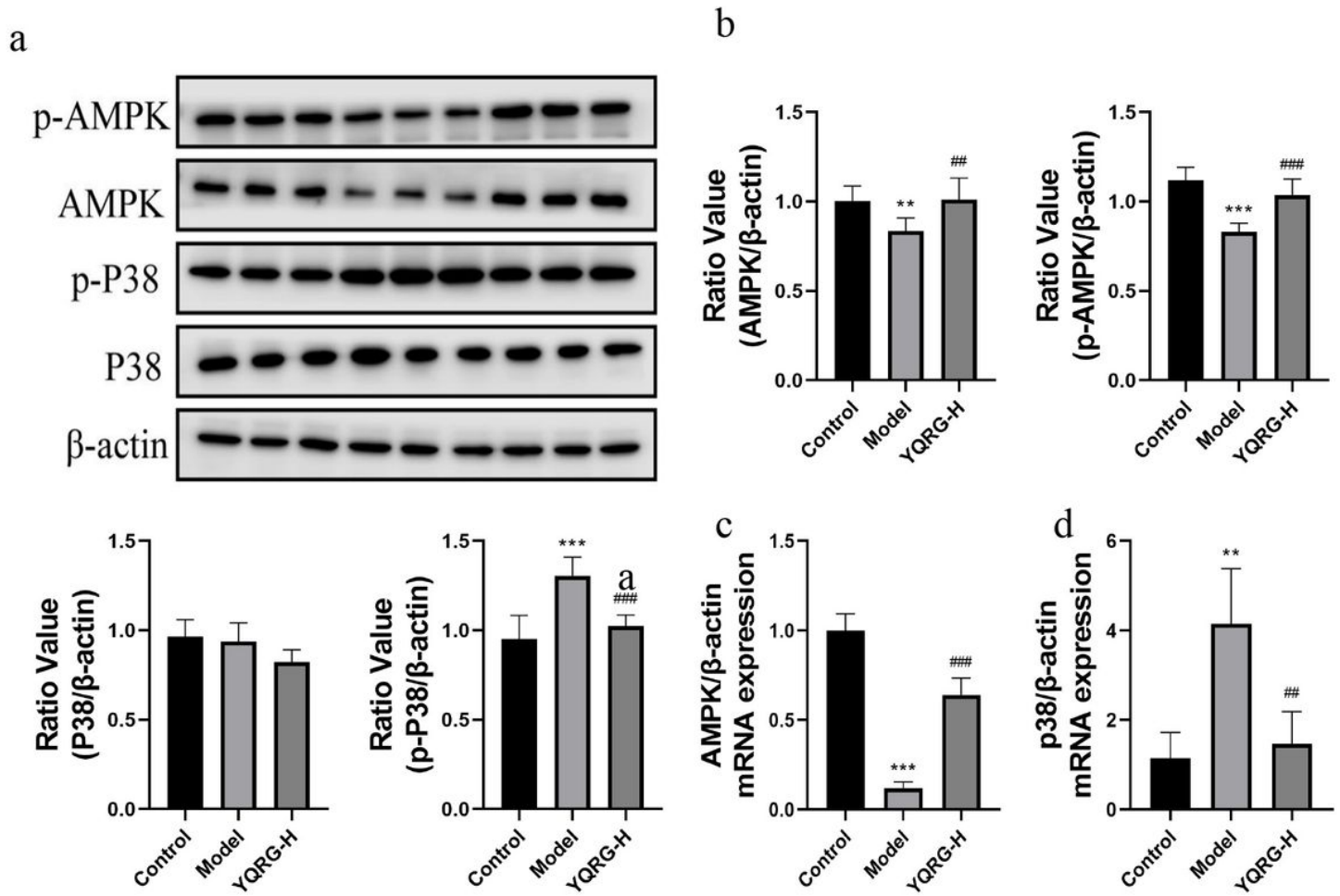

Figure 9

Effect of YQRG on the P38MAPK and AMPK signaling pathways. (a) Protein expressions of P38、P-P38、AMPK and P-AMPK were determined by Western blotting. (b) Protein concentration analysis. (c-d) mRNA expression of P38, AMPK were detected by PCR. Data values were indicated as mean ± SD. *P < 0.05, **P < 0.01 ,***P < 0.001, vs. control group; #P < 0.05, ##P < 0.01, ###P < 0.001, vs. model group